Incorporating geometric detector properties into three-dimensional optoacoustic tomography

Daniel Queirós*[a,b,c], Xosé Luís Déan-Ben[a,b], Andreas Buehler[a,b], Daniel Razansky[a,b], Amir Rosenthal[a,b], and Vasilis Ntziachristos[a,b]

[a]Institute for Biological and Medical Imaging (IBMI), Helmholtz Zentrum München, Ingolstädter Landstraße 1, 85764 Neuherberg, Germany; [b]Chair for Biological Imaging, Technische Universität München, Ismaningerstraße 22, 81675 München, Germany ; [c]TUM Graduate School of Information Science in Health, Technische Universität München, Boltzmannstraße 11, 85748 Garching, Germany

* daniel.queiros@helmholtz-muenchen.de; phone +49.89.3187.4457; fax +49.89.3187.3017

ABSTRACT

The discrepancy between optoacoustic reconstruction algorithms assuming point-like and realistic finite-size transducers causes severe artifacts. Two model-based algorithms accounting for finite-size of cylindrically focused detectors are presented and its performance tested in simulations and experiments.

Keywords: Optoacoustics, photoacoustics, tomography, detector

1. INTRODUCTION

Commonly used piezoelectric transducers in optoacoustic tomographic systems have surfaces with a finite dimension. The finite width of the transducer deviates from the ideal assumption of a point detector, which is employed in typical back-projection reconstruction methods, hence limiting the resolution and quantification achieved [1, 2]. Herein, we examine the effects of the geometrical features of cylindrically focused detectors on the imaging performance achieved by two-dimensional cross-sectional optoacoustic imaging systems. Reconstructed images obtained with two-dimensional inversion are contrasted with images obtained using three-dimensional reconstructions incorporating the geometric detector properties.

2. THEORY

Under assumption of thermal and stress confinement in a uniform acoustic medium, the optoacoustic wave generation is mathematically described by the wave equation Cauchy problem

$$\frac{\partial^2}{\partial t^2} P(x,t) - c_s^2 \nabla^2 P(x,t) = 0 , \tag{1}$$

$$P(x,0) = \Gamma f(x) , \tag{2}$$

$$\frac{\partial}{\partial t} P(x,0) = 0 , \tag{3}$$

which has as an explicit solution

$$P(x,t) = \frac{\Gamma}{4\pi} \iiint \frac{\partial}{\partial t} \frac{\delta(|x-x'| - c_s t)}{|x-x'|} f(x') dx' . \tag{4}$$

Here $P(x,t)$ is optoacoustic pressure, Γ the Grüneisen Parameter, c_s is speed of sound and $f(x)$ is the spatial distribution of the absorption of the excitation light energy pulse. Model-based reconstruction consists of a numerical discretization followed by algebraic inversion of Eq. 4, implemented herein with the interpolated model-matrix inversion algorithm (IMMI) [3, 4]. Thereby, the pressure at a given point and at a given instant is expressed as a linear combination of the absorption in the pixels (two-dimensional case) or voxels (three-dimensional case) of the reconstructed region of interest (ROI). This leads to the matrix-vector equation given by $\tilde{P} = M \cdot \tilde{f}$, with vector $\tilde{P}$ corresponding to the pressure at a set of positions and instants, vector $\tilde{f}$ corresponding to the optical absorption per unit volume at the points of the ROI. M is termed the model-matrix, which establishes the relationship between deposited optical energy and detected pressure waves. Due to the sparsity of M, the inversion can be implemented with high efficiency by using the LSQR algorithm, which calculates the solution $\tilde{f}_{sol}$ given by $\tilde{f}_{sol} = arg\min_{\tilde{f}} \left\| \tilde{P} - M \cdot \tilde{f} \right\|^2$.

Eq. 4 calculates the optoacoustically generated pressure waves detected at a single position in space (point detector assumption). The signal $P_{det}(x_c, t)$ collected by an actual transducer can be estimated as the averaged pressure on its active surface S, i.e.

$$P_{det}(x_c, t) = \iint_S P(x', t)\, dx', \tag{5}$$

where x_c is the center of the detector. In this work, we analyze two different approaches to model the shape of the transducer. The first approach approximates the surface of the transducer by a set of surface elements with positions $x_S \in S$ (Fig. 1a) and size Δx_S. Thereby, Eq. 5 is approximated by $P_{det}(x_c,t) \approx P_{sum}(x_c,t) = \sum_{x_S \in S} P(x_S,t) \cdot \Delta x_S$.

The second approach considered is based on analytically calculating the spatial impulse response (SIR) $h(x,x',t)$ of a line transducer [5]. Here t is time, x location of the center of the line (detector) and x' position of a point source. Thereby, the cylindrically focused detector can be approximated by n lines (centered at $x_1, \cdots, x_n$; Fig. 1b) and its impulse response $h_{det}(x,x',t)$ can be estimated as

$$h_{det}(x_c, x', t) \approx \sum_{i=1}^{n} h(x_i, x', t), \tag{6}$$

where $h(x_i, x', t)$ is the impulse response of each of the lines. The detected signal collected by the transducer is then given by

$$P_{det}(x_c, t) \approx \frac{\Gamma}{4\pi} \iiint \left[h_{det}(x_c, x', t) * \frac{\partial}{\partial t} \delta(t) \right] f(x') dx', \tag{7}$$

where $*$ represents temporal convolution. In both cases one obtains a new model matrix for inversion (M_{sum} or M_{det}) incorporating the geometric properties of the transducer.

3. SIMULATIONS AND EXPERIMENTS

Numerical simulations were employed to examine the accuracy of both models described above. An optical absorption distribution $f(x,y,z)$ corresponding to three-dimensional truncated paraboloids with radius r_0 was taken. For this absorption pattern, the laser-induced pressure wave detected at a point in space can be calculated analytically and the analytical signal for an entire detector surface was approximated by summing up the signals calculated at over 2000 equidistant points on the transducer surface. Both in simulations and experiments a cylindrically focused transducer with a circular shape was considered (see Fig. 1c). The diameter of the circle is 1.3 cm and its focal length is 2.54 cm.

Both proposed surface discretizations predicted signals that were almost identical to the ones calculated analytically (Fig. 2b and 2c). This held also true for a stack of cross-sectional images of a mouse. Here, again, the two model matrices, M_{sum} and M_{det}, were multiplied by the stack of images and yielded identical signals in the time (Fig. 2e) and frequency domain (Fig. 2f). As the two models showed the same behavior, model matrix M_{det} was considered in the rest of the simulations due to the lower computational time for wide detectors.

Then analytical signals were calculated for a tomographic geometry considering a cylindrically focused transducer scanned along a circumference surrounding the object with a 2.25° step (160 projections) and additionally scanned linearly along 0.6 cm in longitudinal direction (31 steps), so that 4960 transducer positions are taken (Fig. 3). The inversion was performed using two alternative methods. First, a 2D-model matrix representing the 160 detector positions in one plane was calculated. Thereby each plane was reconstructed separately with this matrix, resulting in a stack of 2D-reconstructions representing the volumetric ROI. Second, the full 3D-model matrix incorporating the SIR of the transducer was calculated and inversion done once for the entire 3D ROI.

Four small parabolic absorbers with radius r_0 = 200 µm (Fig. 4a and d) were placed in the middle plane, starting from the center going outward. The reconstruction achieved by inverting a 2D model for each plane shows the expected smearing of the absorbers moving out of the center of the image (Fig. 4b). This is due to the assumed point transducers in the model which do not correspond to the actual signals collected by the transducers. Also, reconstructed absorption values are severely damped resulting in significant quantification errors. Smearing over almost the entire ROI is observed in the z-direction, corresponding to strong out-of-plane artifacts (Fig. 4e). On the other hand, the reconstruction retrieved with the full 3D model including the SIR of the detectors significantly reduced the smearing in the out-of-plane (Fig. 4f, 4h, 4i) and in-plane directions (Fig. 4c, 4g). Resolution in all spatial dimensions was improved with the 3D model incorporating the SIR of the transducer.

The procedure suggested in this work was also tested in experiments with agar phantoms containing an ex vivo spleen of a mouse. The cylindrical phantoms with a diameter of 2 cm were prepared using a gel made from distilled water, containing Agar (Sigma-Aldrich, St. Louis, MO, USA) for jellification (1.3% w/w) and an Intralipid 20% emulsion (Sigma-Aldrich, St. Louis, MO, USA) for light diffusion and more uniform illumination (6% v/v), resulting in a gel presenting a reduced scattering coefficient of $\mu_s^{'} \approx 10$ cm^{-1}. The agar phantom containing the mouse spleen was measured with a high throughput optoacoustic tomographic system described in detail in [6]. Here, the signals are collected with a transducer array. It covers 172° with 64 cylindrically-focused elements. The size of the elements is approximately 2mm and 15mm in the azimuthal and elevational directions. Due to the small width of the elements as compared to their height, the main effect in the reconstructions was the out-of-plane spreading of the absorbers. Thereby, the modeling of the transducer in this case was simplified by discretizing it with 150 surface elements in the elevational direction and neglecting azimuthal extensions. An improvement in the elevational resolution is obtained with the 3D model as shown in the maximum intensity projection (MIP) along the y direction (Fig. 5b and d). The reduction of the out-of-plane artifacts corresponding to low spatial frequencies also improves the visual quality of the MIP along the z direction. The overall background noise observed in the 2D reconstruction (Fig. 5a) was considerably reduced in the 3D reconstruction (Fig. 5).

4. DISCUSSION

In this work we adapted a model-based reconstruction algorithm to account for the effects of cylindrically focused transducers in tomographic optoacoustic reconstructions. It was shown in the simulations that the in-plane smearing observed in two-dimensional reconstructions assuming point transducers can be accounted for when employing the complete three-dimensional model, even for absorbers located at a relatively large distance from the center of the region of interest. Likewise, out-of-plane smearing was also reduced. Overall, the showcased good performance of the methods anticipates its convenience in those cases where high resolution and quantitative optoacoustic tomographic imaging is wanted. Typical artifacts in optoacoustic tomography resulting from data collected by currently used ultrasonic transducers could be efficiently and thoroughly corrected.

REFERENCES

[1] M. Xu and L. V. Wang, "Universal back-projection algorithm for photoacoustic computed tomography," Phys Rev E Stat Nonlin Soft Matter Phys, vol. 71, p. 016706, Jan 2005.

[2] L. A. Kunyansky, "Explicit inversion formulae for the spherical mean Radon transform," Inverse Problems, vol. 23, pp. 373-383, Feb 2007.

[3] A. Rosenthal, D. Razansky, and V. Ntziachristos, "Fast Semi-Analytical Model-Based Acoustic Inversion for Quantitative Optoacoustic Tomography," Ieee Transactions on Medical Imaging, vol. 29, pp. 1275-1285, Jun 2010.

[4] X. Dean Ben, A. Buehler, V. Ntziachristos, and D. Razansky, "Accurate model-based reconstruction algorithm for three-dimensional optoacoustic tomography," Medical Imaging, IEEE Transactions on, vol. PP, pp. 1-1, 2012.

[5] A. Rosenthal, V. Ntziachristos, and D. Razansky, "Model-based optoacoustic inversion with arbitrary-shape detectors," Medical Physics, vol. 38, pp. 4285-4295, Jul 2011.

[6] A. Buehler, E. Herzog, D. Razansky, and V. Ntziachristos, "Video rate optoacoustic tomography of mouse kidney perfusion," Optics Letters, vol. 35, pp. 2475-2477, Jul 15 2010.

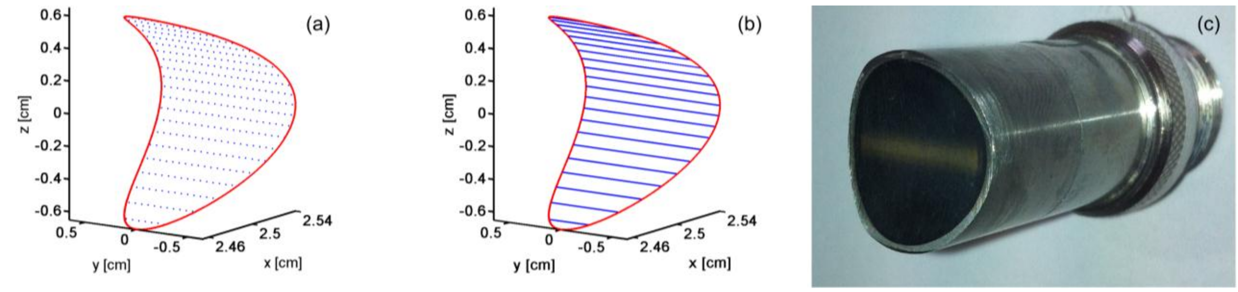

Figure 1: Discretization of a cylindrically focused transducer surface by points (a) and lines (b). (c) shows the transducer used in experiments.

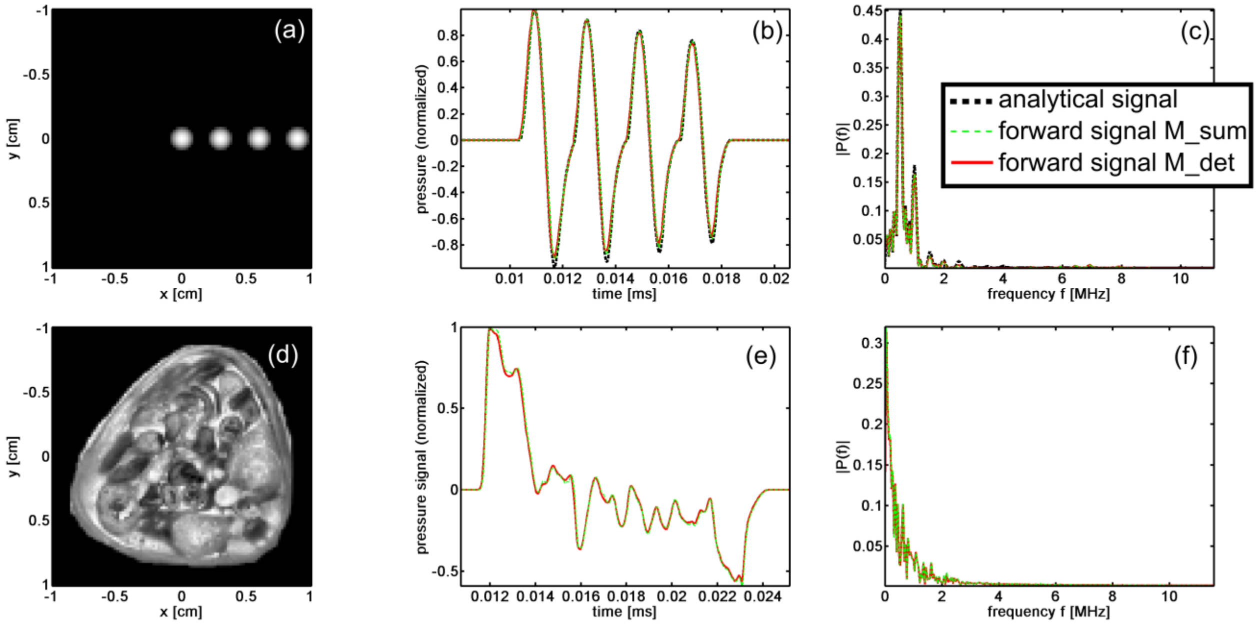

Figure 2: Middle plane of a volume containing four spherical absorbers with a parabolic absorption pattern (a) and their signals predicted by the two different model matrices incorporating geometric detector properties (b). Caption (c) shows the Fourier transform of the time signals. In (d) the cross section of a mouse is depicted. (e) and (f) show correspondingly the signals predicted by the two models and their Fourier transform.

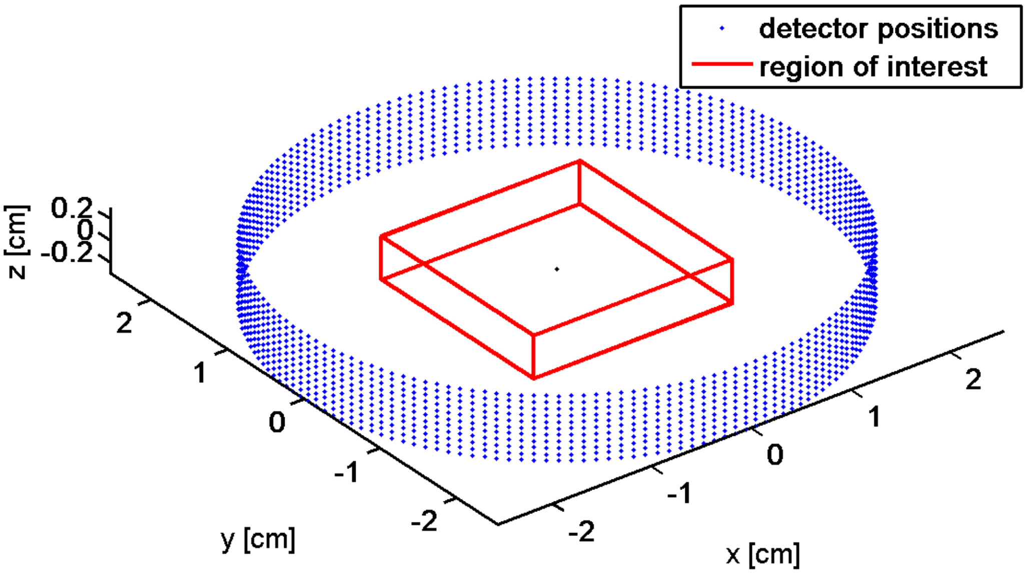

Figure 3: Scanning geometry

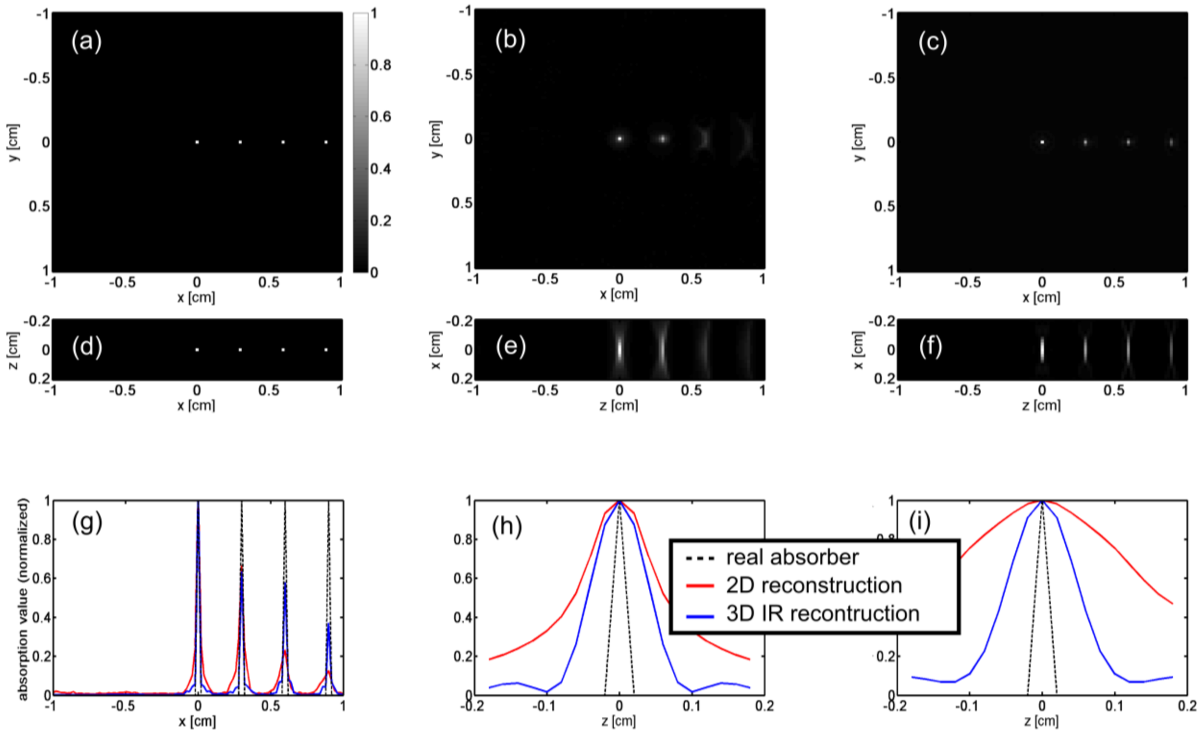

Figure 4: Simulation of 4 absorbers with radius r_0 = 200 µm (a and d) placed along the x-axis in the center of the region of interest. Caption b shows the maximum intensity projection (MIP) along the z-axis of the stack of 2D-reconstructions and caption e its MIP along the y-axis. Caption c depicts the MIP along the z-axis of the 3D reconstruction taking the spatial impulse response of the transducer into account and its MIP along the y-axis (f). Absorption values (normalized) along the x-axis in the middle plane are shown in caption g. Relative improvement of the absorption values in z-direction is shown for the central absorber (h) and the outmost absorber (i).

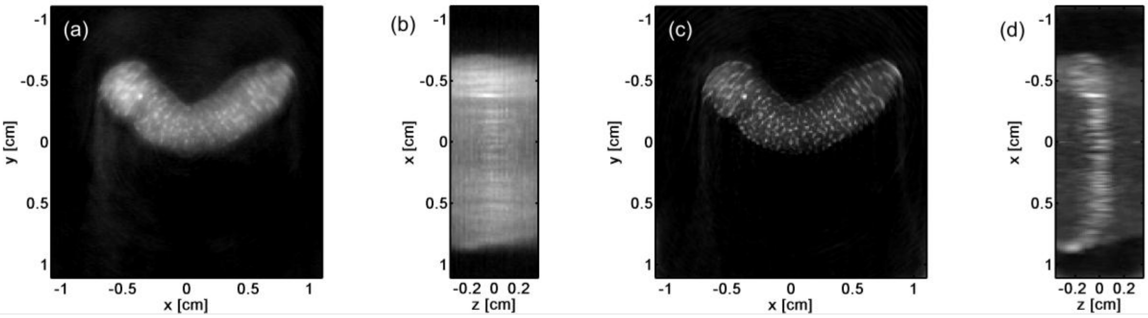

Figure 5: Reconstruction of a mouse spleen. Captions a and b show maximum intensity projections obtained via a 2D model assuming point detectors. Captions c and d are the corresponding reconstructions from the 3D model with the detector properties incorporated.